

# Beyond Residence Time: Quantifying Factors that Drive the Spatially Explicit Filtration Services of an Abundant Native Oyster Population

M. W. Gray<sup>1</sup> D. Pinton<sup>2</sup> · A. Canestrelli<sup>2</sup> · N. Dix<sup>3</sup> · P. Marcum<sup>3</sup> · D. Kimbro<sup>4</sup> · R. Grizzle<sup>5</sup>

Received: 5 March 2021 / Revised: 11 October 2021 / Accepted: 14 October 2021 / Published online: 6 November 2021 © Coastal and Estuarine Research Federation 2021

#### Abstract

The Guana-Tolomato-Matanzas (GTM) system is a well-flushed estuary in Northeastern Florida, USA, and characterized as having an extraordinarily high abundance of oysters that resembles the populations described by Euro-American settlers. Historically, dense populations of oysters, such as those found in GTM, are believed to play an important role in water filtration; however, most research teams seeking to simulate this role have not had access to such robust populations to parametrize their models. To quantify the filtration service (FS) of Eastern oysters (Crassostrea virginica) in GTM at several spatial scales (i.e., reef, watershed, estuary), we implemented a model that solves for the hydrodynamics and depletion of particulate matter passing over model oyster populations, the latter of which were derived from detailed bay-wide surveys. The model results suggested that oyster reefs populating the GTM play an important role in water quality by filtering ~60% of the estuary's volume within its residence time. Our approach teases apart the role of reef size, residence time, particle concentration, and other physical factors on the generation of FS at different spatial scales. Downstream effects were found to be very important for estuary FS, which depend on the spatial distribution of the reefs in the GTM and local and estuarine-scale hydrodynamics. Therefore, the difference between "realized" FS and the "potential" FS of a given reef may be substantial when considering the complex hydrodynamic and connectivity among populations at several scales. Our model results provide clear and actionable information for management of these oyster populations and conservation of their ecosystem services.

 $\textbf{Keywords} \ \ Oysters \cdot Reefs \cdot Crassostrea \ virginica \cdot Ecosystem \ services \cdot Modeling \cdot Delft 3D$ 

# Introduction

Oyster conservation and restoration are often motivated by the suite of ecosystem services thought to accompany robust populations. For example, oyster reefs are widely recognized as an important nursery ground for commercially

Communicated by Nathan Geraldi

- M. W. Gray matthewwgray@gmail.com
- UMCES Horn Point Laboratory, Horns Point Rd, Cambridge, MD 21601, USA
- Dept. of Civil and Coastal Engineering, University of Florida, Gainesville, FL 32611, USA
- Guana Tolomato Matanzas National Estuarine Research Reserve, 505 Guana River Road, Ponte Vedra Beach, FL 32082, USA
- Dept. of Marine and Environmental Sciences, Northeastern University, Boston, MA, USA
- Dept. of Biological Science, University of New Hampshire, 46 College Road, Durham, NH 03824, USA

and ecologically valuable species (Atlantic States Marine Fisheries Commission 2007; Coen et al. 2007; Coen and Humphries 2017). The filtration services (FS) that extend from the suspension-feeding activity of oysters are also highly sought after. As oysters feed, they remove suspended microparticulate material (~2–100 μm) from the water column (Newell and Langdon 1996), improving water quality and clarity. Additionally, the by-products of their feeding activity (feces, pseudofeces, and urea) aid in benthic-pelagic coupling and nutrient cycling, and facilitate denitrification. Recognizing the numerous benefits of oyster FS, top-down control of primary production, and improved water quality is a frequently stated ecological goal of oyster restoration (Mann and Powell 2007), especially in eutrophic estuaries and bays (Cranford 2019). Due to the substantial investment required for large-scale restoration or long-term conservation (Hernández et al. 2018), ecosystem models have become an increasingly popular tool to predict the ecological outcomes prior to any efforts.

Several notable ecosystem models have been developed over the past few decades to describe the role of oysters in controlling primary production. As models achieve greater



sophistication, there has been greater emphasis to use the more ecologically realistic values for how oyster reefs interact with the overlying environment during their parameterization. It is important to note how the ecological modeling community has evolved while also acknowledging some remaining deficits. One important ecophysiological trait to account for during model creation is the role of environmental conditions on oyster filtration activity. Many laboratory studies have demonstrated oysters express elevated filtration rates under optimal laboratory conditions. Early modeling attempts used these elevated feeding rates (e.g., Newell 1988; Gerritsen et al. 1994), but subsequently have been criticized for their lack of ecological accuracy (Pomeroy et al. 2006, 2007; Mann and Powell 2007; Cranford et al. 2011). Oysters living in the dynamic conditions found in estuaries often feed at slower and at more variable rates over time than those found in many laboratory studies (Grizzle et al. 2008; Cranford et al. 2011); thus, in situ-based feeding rates are considered by some to reflect realized rates (e.g., Jacobs et al. 2015; Gray and Langdon 2018) and, thus, arguably more appropriate when modeling the effects of large populations on water quality (but see recent advanced mechanistic models by Saraiva et al. 2017 or Filgueira et al. 2016). Furthermore, there are few examples of water filtration data that extend from fully mature reefs because most native populations are functionally extinct (Beck et al. 2011), and even the stated goals for "restored" populations are far less dense (e.g., Allen et al. 2011) than the enormous and pristine populations described in early accounts by Euro-American settlers (Kurlansky 2007) or models reconstructing their demographics (Mann et al. 2009).

Aside from biological constraints on oyster FS, it is critically important to account for and incorporate hydrodynamics during model creation. Many previous biofiltration models have simplified the hydrodynamics and assumed these systems to be well-mixed and homogenous. However, accounting for mixing, heterogeneous water flow over reefs, and refiltration of water by oysters over time allows for a more precise estimate of time that oysters have to remove suspended material from the water column (Pomeroy et al. 2006; Fulford et al. 2007). Improved estimates of water exposure to oysters can lead to substantially different estimates of FS provided by oyster reefs. For example, Gray et al. (2019) estimated native Olympia oysters to filter 28% of Yaquina Bay, OR within a single residence time after accounting for hydrodynamics. This estimate is substantially larger than that of an earlier study (1% per residence time) by zu Ermgassen et al. (2013a) who used a much simpler method when accounting for hydrodynamics (tidal prism method), which likely underestimated the residence time of the ecosystem (Lemagie and Lerczak 2015). Aside from residence time, the frequency at which a parcel of water was exposed to filter-feeding activity of oysters before exiting

the estuary, termed encounter rate by Gray et al. (2019), was also considered to be important when estimating oyster FS but was not quantified. Water that repeatedly encounters oysters increases opportunity for refiltration by downstream reefs, but this effect can only be accounted for after knowing the precise location of oyster reefs and hydrodynamics.

The approach one uses to estimate spatially explicit oyster FS can also have a direct impact on the resulting estimates. Generally, larger populations will often filter greater quantities of water than smaller ones, which does not provide much insight on the quality and relative services provided by subpopulations. Accounting for the area of populations when estimating FS enables one to determine which populations/locations are more efficient at removing seston. Furthermore, since filtration rates are non-linearly driven by the size of animals (i.e., dry tissue weight; DTW) and bound to be affected by density, reefs of similar area can have vastly different FS if they differ in terms of demographics. For most estuaries, detailed surveys of populations (especially historic ones) are lacking and demographic information is coarse, so assumptions about animal size and reef density during model formulation are derived from generalized relationships found in the literature (e.g., Mann et al. 2009; zu Ermgassen et al. 2013a, b). Accounting for the patchiness common among oyster reefs and demographics can help resolve ecosystem-scale FS and identify populations/locations that are more efficient at particle removal. Such information would greatly aid resource managers prioritizing reefs for conservation and/or developing restoration strategies that maximize return on FS after investment.

To better understand the role of oysters in exerting topdown control over primary productivity, more resolved models at ecosystem scales that account for hydrodynamics and oyster-environmental interactions are needed. The objective of this study was to quantify the filtration services of oysters in Guana-Tolomato-Matanzas River Estuary (GTM hereafter) in Northeastern Florida, USA. A model was created by exploiting recent advances in both biomonitoring and hydrodynamic characterization in the GTM. The GTM is home to an expansive population of Eastern oysters, Crassostrea virginica. In fact, high-resolution surveys of reef boundaries and reef demographics have determined subpopulations to be very dense (mean reef density = 1855 individuals m<sup>-2</sup>). Furthermore, the overall coverage of oysters within the intertidal and subtidal portion of the GTM estuary is small (4% of wet area), but due to the high density of animals found in reefs, the average density of oysters across the area of the estuary (50.7 oysters m<sup>-2</sup>) is among the higher estimates of historical populations (1880–1910) across the Atlantic Coast (range: 1.5-57.5 individuals m<sup>-2</sup>; zu Ermgassen et al. 2013b). The GTM oyster population is pristine itself as there are signs of anthropogenic impacts among many



subpopulations (e.g., high mortality associated oysters in wake zones); however, its robust densities and coverage resemble pre-colonial population estimates (Mann et al. 2009). Therefore, modeling the filtration services of this population could provide insight about the role oysters historically played in many US estuaries.

# **Methods**

# **Study Site**

The GTM National Estuarine Research Reserve (GTM-NERR) spans 60 km north and south of the city of St. Augustine in Northeastern Florida (Fig. 1), at the transition between subtropical and temperate climates. The GTM estuary is primarily fed from the Atlantic Ocean through

the St. Augustine inlet (29° 91' N, 81° 29' W) and Matanzas inlet (29° 71′ N, 81° 23′ W). It is traversed north-south by the Intracoastal Waterway (ICW) through the Matanzas and Tolomato Rivers. The absence of major freshwater rivers makes the estuary well mixed and well flushed (Sheng et al. 2008). The three largest tributaries are Pellicer Creek, which empties into the Matanzas River in the southern portion of the estuary, San Sebastian River, which flows through the city of St. Augustine and empties into the Matanzas River, and Guana River, the northern reaches of which were impounded in the mid-1950s. Other minor tributaries are the Moultrie Creek and Moses Creek, which empty into the Matanzas River ~9 and ~17 km south of St. Augustine. The average tidal range in the estuary is ~1.5 m (NERRS 2021). Salinity varies from near zero ppt in the tributaries to 25–35 ppt near the inlets (NERRS 2021). Water temperature typically ranges from 15 to 30 °C (NERRS 2021). Dominant

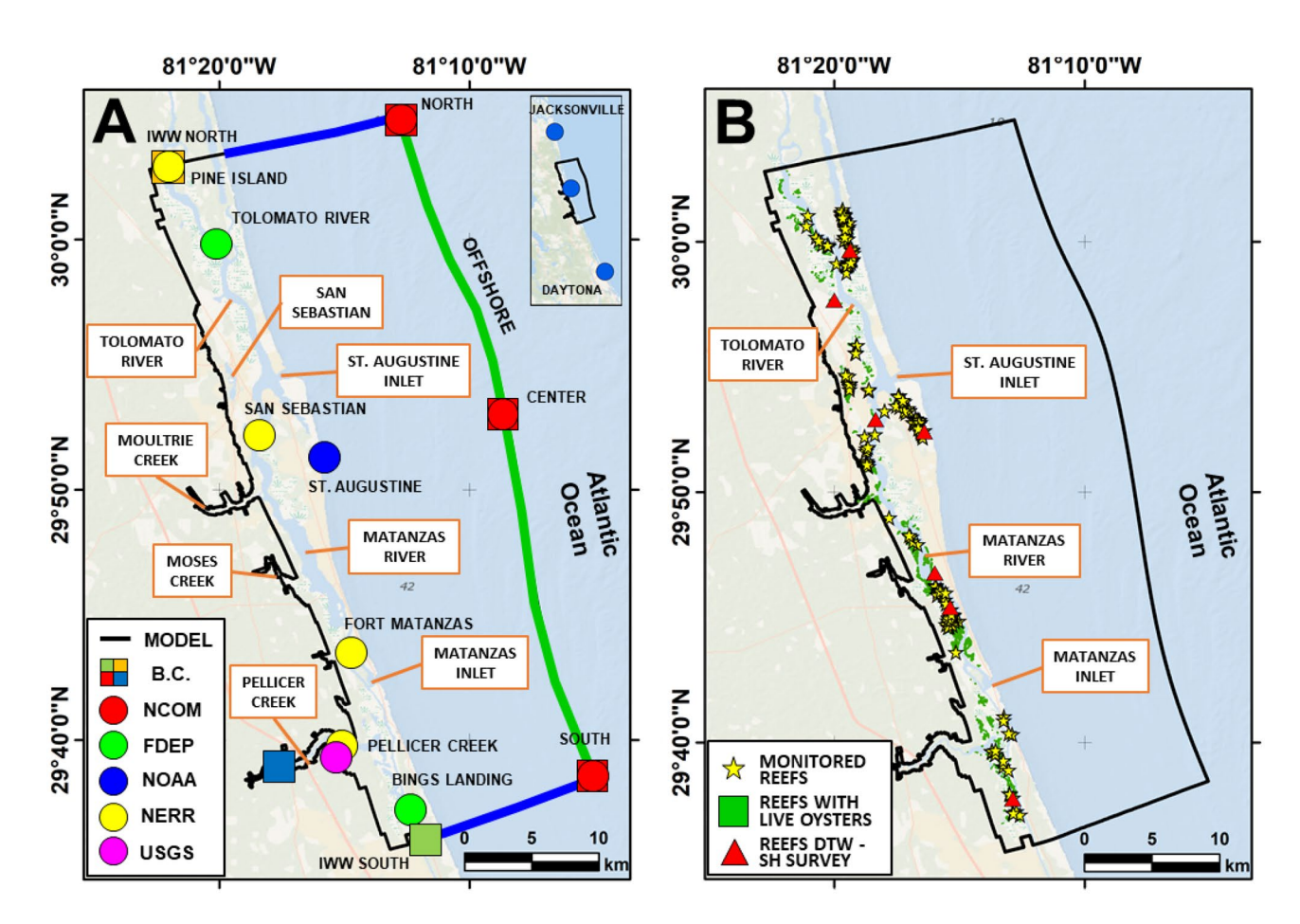


**Fig. 1** A The geographic position of the data sources (stations and numerical model points) used to determine the boundary conditions for our simulations (dots), and the geographic position of the open boundaries of the model domain (squares). The red dots indicate the locations where we extracted the boundary conditions for the water temperature. The other dots indicate the FDEP, NOAA, and NERR stations where we extracted the hydrodynamic boundary conditions. **B** Spatial distribution of the oyster reefs in the GTM estuary.

Green areas indicate the reefs extracted from the Fish and Wildlife Research Institute (FWRI) database (https://hub.arcgis.com/datasets/myfwc::oyster-beds-in-florida), which are populated by live oysters. The yellow stars indicate the reefs surveyed by the GTMNERR. The red triangles indicate the reefs where we surveyed DTW and SH, to determine a relationship between them. In all plots, the black line represents the model domain



habitats in the estuary include salt marshes, mangroves, intertidal oyster reefs, tidal creeks, mudflats, and open water (Dix et al. 2017, 2019; Bacopoulos et al. 2019). Intertidal habitats are protected from ocean energy by barrier islands and dune systems.

# **Hydrodynamic Model Details**

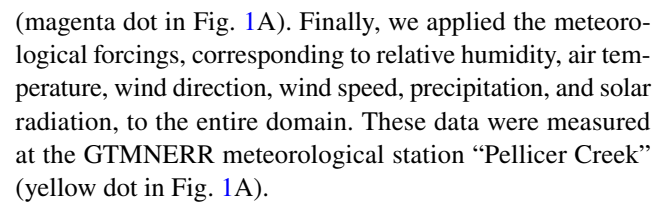
We solved the hydrodynamics and the temperature exchange in the GTM estuary by using the Delft3D-FLOW model (https://oss.deltares.nl/web/delft3d/download—see Supplementary Material (SM): S1). It calculates non-steady flow resulting from the tidal and meteorological forcing on a regular, boundary-fitted grid. In this study, we used a structured curvilinear grid that covers an area of ~1050 km<sup>2</sup>.

The model domain (Fig. 1, black line) envelops the GTM-NERR and was centered in the city of St. Augustine, FL, USA. The numerical grid describes the following: (i) the GTM estuary, composed of the ICW and the Guana River up to the Guana Dam; (ii) the principal and minor affluents of the GTM in the study area (see the "Study Site" section); (iii) the Atlantic Ocean, up to ~12 km from the coastline; and (iv) the inlets of St. Augustine and Matanzas. The average grid cell dimension varied from ~30 m × 100 m in the ocean to ~15 m × 20 m in the estuary.

The model bathymetry for the ocean was based on the National Oceanic and Atmospheric Administration (NOAA) data. The bathymetry for the GTM was based on the Florida Natural Areas Inventory (FNAI) vegetation map (https://www.fnai.org/LandCover.cfm), the United States Geological Survey (USGS) bathy LiDARs, the United States Army Corps of Engineers topo-bathy LiDARs, and the NOAA LiDAR datasets (https://coast.noaa.gov/dataviewer/#/).

For this study, we simulated a period of 30 days, which contained ~2 neap and ~2 spring tides (see SM: S2). The simulated period lasted from May 9, 2018, to June 10, 2018. The simulation time step was 1 min.

At the offshore boundary, we forced the simulation (green lines in Fig. 1A) with the harmonic constituents of the astronomical tide measured at three local NOAA stations (see SM: S3, and blue dots in Fig. 1A), and the water temperature extrapolated from the Regional Navy Coastal Ocean Model (NCOM-red dots in Fig. 1A). At the southern boundary of the ICW (green square in Fig. 1A), we applied the water level and the water temperature measured by the Florida Department of Environmental Protection (FDEP) at the "Bing's Landing" station (green dot in Fig. 1A). At the northern boundary of the ICW (orange square in Fig. 1A), we applied a Neumann boundary condition for the water level, and the water temperature measured by the GTMN-ERR at the "Pine Island" station (yellow dot in Fig. 1A). At Pellicer Creek (blue square in Fig. 1A), we applied the tidally filtered discharge rate from the local USGS station



To calculate the distribution of the residence time and the FS in the estuary, we interpolated the model statistics obtained for the simulated period on a uniform  $50 \text{ m} \times 50 \text{ m}$  grid. The statistics we considered were the mean, minimum, and maximum water depth and the depth-averaged water temperature.

# **Oyster Reefs**

# **Field Surveys and Allometric Functions**

We used the Fish and Wildlife Research Institute (FWRI) database (https://hub.arcgis.com/datasets/myfwc::oysterbeds-in-florida) to identify the geographic properties of the oyster reefs in the GTM estuary. Clipped to the study area boundary, the database contained ~4300 reefs divided into two classes: alive and dead. In this study, we considered only the live reefs (Fig. 1B). Detailed surveys were conducted between 2014 and 2020 by the GTMNERR to measure oyster population metrics (i.e., shell height and oyster density) over a sample of ~240 reefs (yellow stars in Fig. 1B). The survey methods are described in Marcum et al. (2018) and are reported in Supplementary Material (S4).

Using the oyster dataset, we calculated the average oyster density  $(D_{Oys})$  and shell height (SH) for each surveyed reef. These parameters correspond to the number of animals per reef square meter and the average length of their shell in millimeters. We used ArcGIS to calculate their values on the not-surveyed reefs by using an inverse distance weighted (IDW) interpolation method. IDW predicts the values for the unsurveyed reefs by using the surrounding surveyed locations.

Filtration rates were dependent on the average dry tissue weight (*DTW*) of oysters in a given reef. Mean *DTWs* were derived from relationships between *DTW* and *SH* from surveys conducted at seven stations distributed throughout the estuary (Fig. 1B). Specifically, in June 2018, we haphazardly sampled three reefs separated by at least 10 m within each station (21 reefs total), yielding three oysters within ten different *SH* size classes (i.e., range 0 to 100 mm at 10 mm intervals) at each station. Oysters were cleaned of all epifauna, frozen, and then transported to Northeastern University for processing: oyster *SH* was determined by measuring the length (mm) of the longest bottom valve axis from ubmo to tip; *DTW* was quantified by shucking oysters, separating tissue from shell, placing tissue tin pre-weighed tin (Metler-Toledo Balance, model MS403S), drying the container at



60 °C for 72 h, re-weighing the tin container, and subtracting pre- and post-dried container weight (g).

Non-linear regression analysis was used to determine that slope estimates between DTW and SH were similar among sites, indicating that a general relationship across estuary was permissible. Using Akaike Information Criterion (Akaike 1973) during non-linear model selection, the following three parameter exponential relationship between DTW and SH was found best to fit the data ( $R^2 = 0.87$ ):

$$DTW = -0.41 + 0.34e^{(0.015 \cdot SH)}$$
 (1)

We then estimated the *DTW* in grams of the average oyster populating each reef using the local average *SH* as determined through surveys and applied it to Eq. (1).

## Physiology

Oyster filtration rate  $(FR_{Oys})$  was defined as the volume of seawater filtered per unit time by each animal ("Oys," m<sup>3</sup> h<sup>-1</sup> oyster<sup>-1</sup>). The methods used here were based on the approach of zu Ermgassen et al. (2013b) to examine the present and historical services of individual oysters along the Atlantic and Gulf Coasts. In their approach,  $FR_{Oys}$  was estimated as:

$$FR_{Ovs} = a \cdot DTW^b, \tag{2}$$

where a is the maximum filtration rate of an individual, and b is a scaling exponent. b describes how filtration scales with the dry tissue weight of animals (DTW, in grams), calculated from the individual shell height using the allometric function proposed by Newell and Langdon (1996). After careful analysis, zu Ermgassen et al. (2013b) set a to 8.02 and b to 0.58. The latter is the universal value for suspension-feeding bivalves (Cranford et al. 2011). To account for the effect of water temperature on the oyster, Eq. (2) was modified using the method proposed by Cerco and Mark (2005) to:

$$FR_{Ovs} = 8.02 \cdot DTW^{0.58} \cdot e^{-0.015(T-27)^2},$$
 (3)

where T is the water temperature in Celsius degrees.

#### **Residence Time Calculation**

To calculate the residence time in the study area, we tracked the motion of virtual particles released in the GTM estuary by using the PART module of Delft3D. To simulate the motion of the particles, Delft3D-PART uses the hydrodynamic fields calculated by the FLOW module. This study employed conservative and neutrally buoyant particles, which were distributed uniformly in the GTM estuary. Particles were injected six times in the estuary,

with a time interval of 2 h between two consecutive injections. This method was used to cover the first tidal cycle and to consider the effect of tidal variability in the motion of the particles. The injection locations were the midpoints of the 50 m  $\times$  50 m regular grid cells, flooded for at least a time step of the hydrodynamic simulation. These cells constitute the wetted area of each watershed (hereinafter: wetted watershed,  $A_W$ ). The wetted area of a watershed is composed of a subtidal portion  $(A_S)$ , which is made of permanently flooded cells, and an intertidal portion  $(A_I)$ , which is flooded only during high water levels. The distribution of  $A_W$ ,  $A_S$ , and  $A_I$  in the GTM is shown in Fig. 2A. The time step we chose for particle tracking was 1 min, consistently with the hydrodynamic model.

In this study, we calculated residence times at three spatial scales: (i) the local residence time  $(RT_L)$ , defined for each 50 m×50 m cell in the estuary, (ii) the watershed residence time  $(RT_W)$ , calculated for the watersheds we identified in the GTM estuary from the FDEP Waterbody ID drainage basin layer (https://geodata.dep.state.fl.us/datasets/ waterbody-ids-wbids), and (iii) the estuary residence time ( $RT_E$ ). The watersheds were identified by aggregating the ~40 watersheds located in the study domain, in nine groups  $(W_1 \text{ to } W_0 \text{ in }$ Fig. 2B), which contain the afferent area of the most important rivers and creeks of the GTM and the two inlets (see SM-S5). To calculate the local residence time, we identified all the particles entering each 50 m $\times$ 50 m cell, and the total time they spent inside the cell throughout the entire simulation. For each cell, the average of these times was the local residence time. The watershed and the estuary residence times were defined as the time needed for the particles to decrease their number by 1/e (with e  $\approx$  2.7) in the watersheds and estuary, respectively. These residence times were computed by considering only the particles released with the first injection.

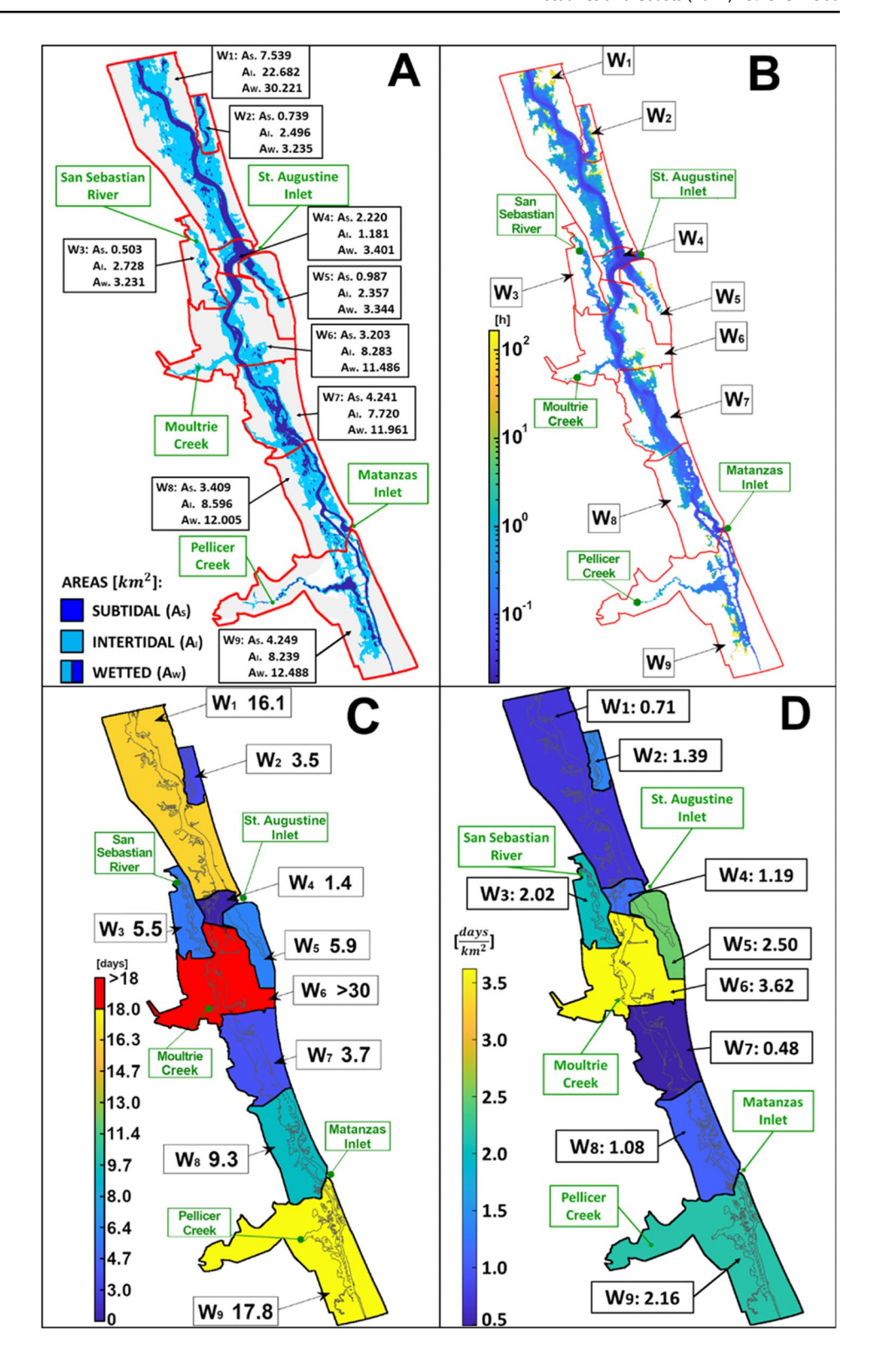
The value of residence time grows with the dimension of the basin. To make  $RT_W$  independent from the basin dimension, we calculated  $RT_W^A$ , which is the watershed-scale residence time per unit of wetted watershed  $(A_w)$ .

#### **Filtration Services Calculation**

Oyster FS were defined as the percentage of water mass filtered in the estuary within a single residence time. FS was computed at the levels of a single reef ( $FS_R$ ), an entire watershed ( $FS_W$ ), and at the estuary scale ( $FS_E$ ). To quantify the contribution of each reef to the estuary-scale FS, we developed a MATLAB code that evaluates interactions between virtual oysters and suspended particles tracked by Delft3D-PART. The code was based on the following assumptions: (i) each particle is initialized with a particle concentration (x) of 1, (ii) at each time step, the concentration of the suspended



Fig. 2 A Distribution of the subtidal  $(A_S)$ , intertidal  $(A_I)$ and wetted (AW, or total) areas calculated for the most important watersheds  $(W_i, i=1,...9)$ constituting the GTM. B Distribution of the local residence time  $(RT_I)$  in the GTM estuary, using a 50 m×50 m regular grid. Times are indicated in hours. The nine watersheds in which we divided the GTM are indicated in red. Note that the residence time is computed for the portion of the watershed that is wet over a spring-neap cycle. C Distribution of the watershed-scale residence times  $(RT_W)$  calculated for the most important watersheds  $(W_i, i=1,...9)$  constituting the GTM. Times are indicated in days. (D) Distribution of the watershed-scale residence time per unit of intertidal watershed  $(RT_{W}^{A_{I}})$ , calculated for the most important watersheds  $(W_i,$ i = 1,...9) constituting the GTM. Residence time is indicated in days/km<sup>2</sup>



particles is reduced by oyster reefs proportionally to a filtration rate, (iii) particles are filtered only when they travel above a reef, and (iv) there is no increase in the concentration of particles above the initial concentration. The method used here was inspired by that of Gray et al. (2019); however, the new approach here substantially improves reef/particle interactions (see Supplementary Materials for greater detail in model approach differences).



In this study, filtration rate of the average oyster populating each of the ~4300 reefs was calculated in the GTM estuary by applying the DTW calculated from Eqs. (1 to 3). To calculate the number of animals populating a reef, we multiplied the local oyster density  $(D_{Oys})$  for the reef area  $(A_R)$ . We then calculated the filtration rate of the entire reef (FR) by multiplying the number of oysters populating it by the filtration rate of a singular animal  $(FR_{Oys})$ :

$$FR = D_{Oys} \cdot A_R \cdot FR_{Oys.} \tag{4}$$

FR is defined as the seawater volume filtered per unit time by an entire reef (m<sup>3</sup> h<sup>-1</sup>). By using Eq. (4), we calculated FR accounting for the spatial distribution of water temperature, oyster density, and oyster dry tissue weight in the GTM estuary.

The concentration reduction (dx) due to oyster filtration of material traveling over a specific reef was described with the following equation:

$$dx = -\frac{x}{V} \cdot FR \cdot dt,\tag{5}$$

where the total concentration of over a reef is x, the volume of water above a reef is V, and dt is the time step of the hydrodynamic and particle tracking simulations (1 min). The water volume on a reef (V) varied at each time step and depended on both the reef elevation and the water level calculated in the cells. Thus, knowing the reef properties and the water depth at any given time step, it was possible to calculate from Eqs. (4 and 5) the fractional change  $(F_{i,k})$  in the mass of the  $i^{th}$  particle over any reef, at any given time stepk. Given the mass  $x_{i,k}$  of the  $i^{th}$  particle at the beginning of the  $k^{th}$  time step, and knowing that the particle is suspended over a reef for that time step, the mass at the beginning of the next time step is:

$$x_{i+1,k} = F_{i,k} \cdot x_{i,k}. \tag{6}$$

The MATLAB code records the amount of particle mass cleared by each reef at each time step. This allowed us to compute the total amount of particle mass removed from the estuary by each reef and to identify the reefs that most contribute to the filtration of the GTM estuary. The proportion of the estuary cleared by a reef  $(FS_R)$  is:

$$FS_R = \frac{\sum_{k=1}^{N_T} \sum_{i=1}^{N_{R,k}} -dx_{i,k}}{\sum_{i=1}^{N_P} x_{i,1}},$$
(7)

where  $N_T$  is the total number of time steps (k) of the particle tracking simulation,  $N_{R,k}$  is the number of particles floating above the reef at a given time step k, and  $N_P$  is the total number of particles injected in the estuary. This definition of filtration services accounts for downstream effects because the  $FS_R$  depends on the filtration history

of each particle. Because of the complex hydrodynamics of the estuary, due to the massive presence of salt marshes (Bacopoulos et al. 2019), and the dominant effect of the tide on the water fluxes (Sheng et al. 2008), the distribution of the downstream effect in the estuary is non-uniform.  $FS_W$ , which is computed as the sum of all  $FS_R$  in a specific watershed, grows with the dimension of the intertidal watershed area, where oyster reefs preferentially develop. Consequently, it is difficult to discern if large watersheds provided a large service because of their size or because of the filtration capability of their reefs. To overcome this issue, we calculated  $FS_W^{A_I}$ , that is the  $FS_W$  per unit of intertidal watershed area  $A_I$ , which reads:

$$FS_W^{A_I} = \frac{FS_W}{A_I} \tag{8}$$

Similarly, the filtration service at the reef scale  $FS_R$  increased with the reef size; thus, it was hard to discern if a large  $FS_R$  indicated a specific ability of the reef to filter water, or it was a consequence of a large reef size. To estimate the relative contribution of each reef to  $FS_W$  and  $FS_E$  independently from their size, we calculated  $FS_R^{A_R}$ , which were the values of  $FS_R$  per unit of reef area  $A_R$ , and itheir watershed-averaged value  $(\overline{FS}_R^{A_R})$ :

$$FS_R^{A_R} = \frac{FS_R}{A_R} \tag{9}$$

$$\overline{FS}_{R}^{A_{R}} = \frac{\sum_{j=1}^{N_{R}^{W}} (FS_{R}^{A_{R}} \cdot A_{R})}{\sum_{j=1}^{N_{R}^{W}} \cdot A_{R}}$$
(10)

where  $N_R^W$  is the number of reefs in the watershed W.

Finally, to separate the contribution of intertidal area and FS per unit of intertidal area, we write:

$$FS_W = A_I \cdot FS_W^{A_I}. \tag{11}$$

Since, by definition, the total area of the reefs in a watershed per unit of watershed intertidal area reads:

$$A_R^I = \frac{\sum_{j=1}^{N_R} A_R}{A_I} \tag{12}$$

we have that  $FS_W^{A_I}$  in Eq. (8) can also be written as:

$$FS_W^{A_I} = \overline{FS}_R^{A_R} \cdot A_R^I. \tag{13}$$

By substituting (13) into (11), we have that:

$$FS_W = A_I \cdot \overline{FS}_R^{A_R} \cdot A_R^I. \tag{14}$$



Equation (14) allows us to evaluate the separate contribution of the watershed intertidal area, the watershed-averaged value  $FS_R$ , and the percentage of  $A_I$  occupied by oyster reefs to the value of the watershed-scale filtration service.

# **Statistical Analysis: Genetic Algorithm**

To define a relationship between the reef-scale filtration services, and the local hydrodynamic, geometrical, and biological variables, we performed a statistical analysis using a Genetic Algorithm (GA) (Madár et al. 2005). The GA simulates a biological evolution process. The process starts with a population of random individuals, which grow at each time step until they reach an optimal solution. The individuals of each generational step are chosen using a fitness function calibrated on a target population. The optimal solution is achieved when significant changes in the individuals constituting the successive generations are negligible.

In this study, the calculated filtration services of the reefs per unit of reef area  $(FS_R^{A_R}, \text{Eq. (9)})$  constituted the target population of the GA. The individuals are the values of  $FS_R^{A_R}$  estimated by the GA for each reef. The changes in the population over the generations were the changes in the linear regression function used by the algorithm to fit the input data; the fitness function was the root mean square error (RMSE).

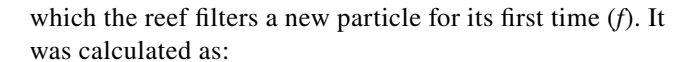
A relationship to describe  $FS_R^{A_R}$  is obtained for each reef by substituting Eqs. (4 and 5) into (7). After some steps, which are reported in SM–S6, we obtain:

$$FS_{R} = \frac{\sum_{k=1}^{N_{T}} \sum_{i=1}^{N_{R,k}} C_{i,k} \cdot FR_{Oys,k} \cdot D_{Oys} \cdot A_{R} \cdot dt}{\sum_{i=1}^{N_{P}} x_{i,1}},$$
(15)

where  $C_{i,k} = \frac{x_{i,k}}{V_k}$  is the concentration of the  $i^{th}$  particle floating above a reef at the  $k^{th}$  time step, and takes into account both the value of  $x_{i,k}$ , and the local water depth (through the volume  $V_k$  of water above the reef at time step k). Equation (15) can then be written as (see SM – S6):

$$FS_{R}^{A_{R}} = \frac{\sum_{k=1}^{N_{T}} \sum_{i=1}^{N_{R,k}} C_{i,k} \cdot FR_{Oys,k} \cdot D_{Oys} \cdot dt}{\sum_{i=1}^{N_{P}} x_{i,1}} \propto N \cdot RT_{R} \cdot \overline{C} \cdot \overline{FR}_{R}^{A_{R}}$$
(16)

In Eq. (16), N is the number of distinct particles entering a reef during the simulation. This means that, even if a particle enters multiple times a reef, its contribution to N is equal to one;  $RT_R$  is the average time spent by the particles on the reefs, which correspond to the reef-scale residence time;  $\overline{FR}_R^{A_R}$  is the average filtration rate of the reef per unit of reef area observed over the time steps in



$$\overline{FR}_{R}^{A_{R}} = \frac{\sum_{f=1}^{N_{F}} FR_{f}^{A_{R}}}{N_{F}},\tag{17}$$

where the total number of these time steps is indicated as  $N_F$ . Finally, in Eq. (16),  $\overline{C}$  is the average concentration  $(C = \frac{x_{i,k}}{V_k})$  of the particles at their first entrance over the reef

Due to their proportionality with  $FS_R^{A_R}$ , we decided to use these values as the predictors of the GA.

Additional predictors we calculated in this study, for each reef, are the following: (i) the local hydroperiod; (ii) the average flow velocity over the reefs; (iii) the local tidal range; (iv) the local tidal prism. However, due to their low statistical significance, we will not return on them hereinafter.

There are many advantages of genetic algorithms over traditional optimization algorithms (Yang et al. 2014): (i) the ability to deal with complex problems; (ii) the possibility to be easily parallelized; (iii) the research of a global and not point solution; (iv) the possibility to deal with various type of optimization; (v) the low sensibility to noisy problems; and (vi) the possibility to be used even with small datasets. Another advantage of the GA is that it gives as output a formulation, which is based on the assigned model predictors. This could be directly adopted for classification procedures and allows an immediate interpretation of the contribution of the model predictors to describe the considered target population. Some limitations of GA are the following: (i) the high computational cost, which is compensated by its possibility to be parallelized, and by our access to the multicore supercomputer "Hipergator" (https://www.rc. ufl.edu/services/hipergator/); (ii) the correct choice of appropriate model predictors, because any inappropriate choice will make it difficult for the algorithm to converge or it will simply produce meaningless results (Yang et al. 2014). This limitation was resolved by using the most informative predictors obtainable from our datasets (see the "Genetic Algorithm" section).

# Results

## **Local Residence Time**

Figure 2B shows the local residence time ( $RT_L$ ) on the GTM estuary. The figure shows that the Guana, Tolomato, and Matanzas Rivers had the lowest residence times, ranging between 1 and 7 min. The lowest  $RT_L$  values, ranging between 1 and 2 min, were observed next to



St. Augustine and Matanzas inlets. These values gradually increased in the major watercourses and reached their maxima at the salt marshes. In these areas, the residence time ranges from 30 to 240 min (0.5–4 h) at the marsh platform to ~2–10 min at the marsh edge. The highest residence times were computed for the marshes farther from the inlets and adjacent to the mainland. In this area,  $RT_L$  reached values up to ~5000–8000 min (~3.5–5.5 days). In addition, the figure shows that  $RT_L$  are relatively higher in the southern than in the northern part of the GTM estuary.

## **Watershed Scale Residence Time**

The watershed-scale residence times  $(RT_w)$  were calculated on the major watersheds of the GTM, described in the "Residence Time Calculation" section and in the Supplementary material (S5), and are shown in Fig. 2C. RT<sub>w</sub> attained its lower value, equal to 1.4 days, for watershed W<sub>4</sub>, which contains St. Augustine inlet (Fig. 2C). A much larger value, equal to 9.3 days, was computed for the watershed  $W_8$ , which contains Matanzas inlet. Higher residence times, equal to 5.5 and 5.9 days, were obtained for the watersheds  $W_3$  and  $W_5$ , which contain the San Sebastian River and Salt Run. Similar values were obtained for watersheds  $W_2$  and  $W_7$ , where  $RT_W$  was equal to 3.5 and 3.7 days, respectively. A greater  $RT_W$  was obtained for the apical and largest watersheds, which are also furthest from the inlets. Watershed  $W_1$ , the northernmost one, containing Tolomato River, had a residence time of 16.1 days. Watershed W<sub>9</sub>, the southernmost one, containing Pellicer Creek, had a residence time of 17.8 days. Finally, watershed W<sub>6</sub>, containing Moultrie River, did not reach the 1/e concentration of the initial number of particles in the 30-day simulation. This is reported in Fig. 3F. Figure 3 shows the temporal variation of the number of particles in the watersheds of the GTM. The number is expressed in percentage with respect to the initial value.

Figure 2D shows the values of  $RT_W$  per unit of intertidal area ( $RT_W^{A_I}$ ) for the watersheds constituting the GTM. In this case, the lowest value, equal to 0.48 days km<sup>-2</sup>, was observed for watershed  $W_7$ , and not for  $W_4$ , which  $RT_W^{A_I}$  is equal to 1.19 days km<sup>-2</sup>. A low  $RT_W^{A_I}$ , equal to 0.71 and 1.08 days km<sup>-2</sup>, was observed also for watershed  $W_1$  and  $W_8$ , respectively. For  $W_1$ , in particular, this is in contrast with its high value of  $RT_W$  (the second highest in the GTM). A slightly higher  $RT_W^{A_I}$  was calculated for  $W_2$ , containing the Guana River. Intermediate values of  $RT_W^{A_I}$  equal to 2.02, 2.50, and 2.16 days km<sup>-2</sup>, were observed for the watersheds  $W_3$ ,  $W_5$ , and  $W_9$ , which included Sebastian River, Salt Run, and Pellicer Creek, respectively. Finally, as for  $RT_W$ , the highest value of  $RT_W^{A_I}$ , equal to 3.62 days km<sup>-2</sup>, was observed for watershed  $W_6$ .

# **Estuary Residence Time**

Figure 4 shows the temporal variation of the particle numbers in the GTM estuary, calculated as a percentage of their initial number. From the numerical simulation, the estuary residence time  $(RT_E)$  was estimated to be 12.6 days.

#### **Filtration Rates**

Physiological rates and other biological traits varied among oyster populations in each watershed (Table 1). Estimates of individual oyster filtration rates ranged from 2.18 to  $3.741\,h^{-1}$  and on average filtered 2.5 l h<sup>-1</sup> (SD: 0.54). After weight-standardizing filtration rates of the small animals (average shell height 35 mm, average *DTW* estimate 0.17 g) that dominated reefs, we estimated that small animals clear on average 13.4 l to 17.5 l h<sup>-1</sup> g<sup>-1</sup> across the estuary. The average weight-standardized filtration rate was 15.9 l h<sup>-1</sup> g<sup>-1</sup> (SD: 1.56).

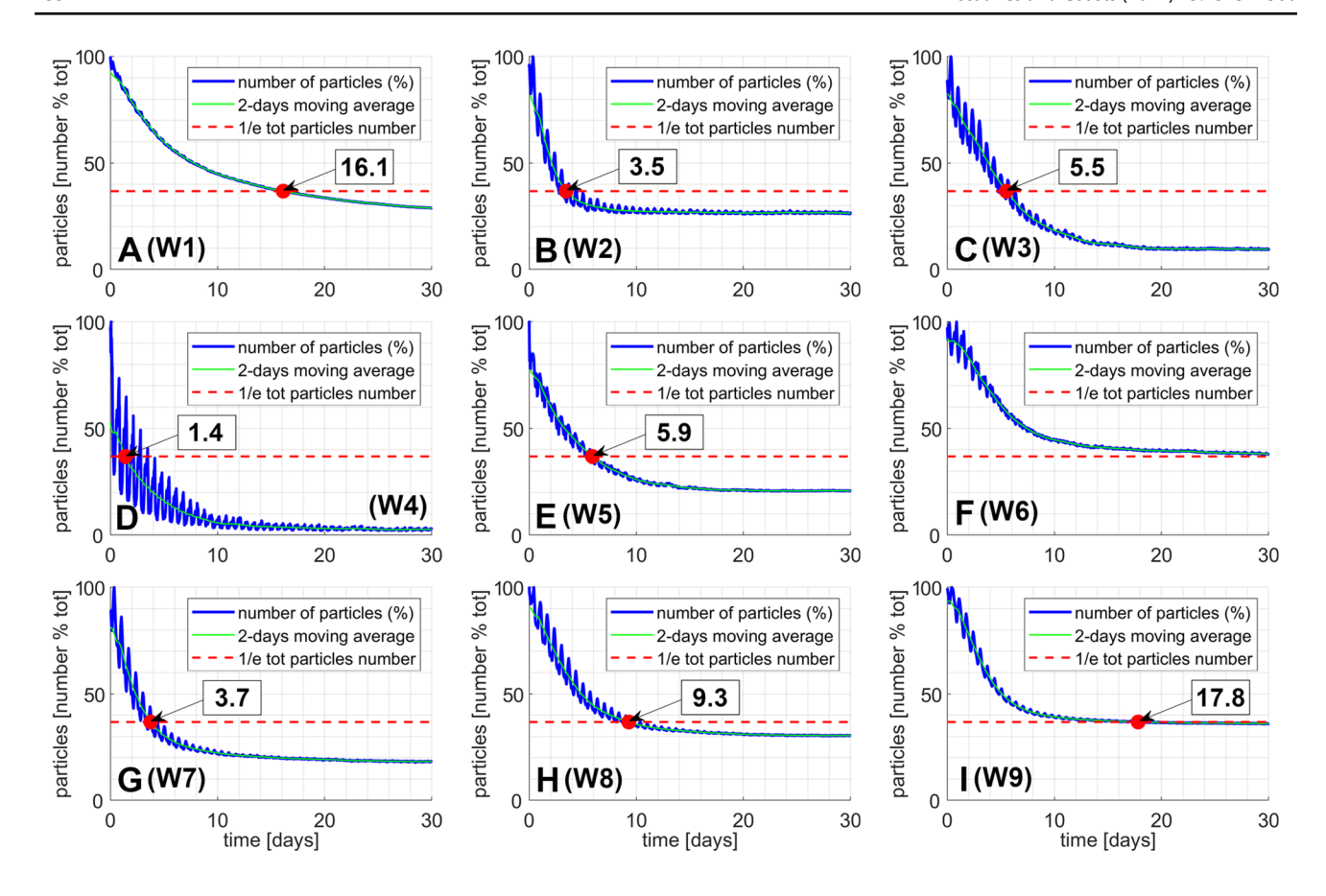
# **Filtration Services**

Figure 5A shows the distribution of the FS calculated at the reef  $(FS_R)$  and watershed scale  $(FS_W)$  in the GTM. The portion of the estuary cleared by a single reef  $(FS_R)$  varied from 0 to 0.90% across the estuary. The total volume of the estuary cleaned by the oyster reefs over an estuary residence time  $(FS_F)$  was ~60%. The greatest contribution to the filtration of the GTM estuary was provided by watershed  $W_1$ (~20% of  $FS_E$ ), followed by the watersheds  $W_6$ ,  $W_7$ , and  $W_8$ , whose  $FS_E$  is 6.07%, 10.12%, and 9.23% respectively. Lower  $FS_F$  values for the watersheds were obtained from  $W_3$ ,  $W_5$ , and  $W_0$ , which provided 1.49%, 2.46%, and 4.16%, respectively. Finally, the lowest  $FS_E$  (0.28%) was obtained for watershed W<sub>4</sub>, containing St. Augustine inlet. In addition, it is important to notice that, after one estuarine residence time, ~22% of the mass initially contained in the estuary, left it from the inlets and the southern and northern boundaries of the ICW. For this reason, the total reduction of mass in the GTM after an estuarine residence time is ~81%.

Figure 5B shows the spatial distribution of  $FS_W$  per watershed area ( $FS_W^{A_I}$ ), expressed in [% km $^{-2}$ ]. The distribution differs from the one observed for  $FS_W$ . Once again, the lowest value (0.23) was observed for the watershed containing St. Augustine inlet ( $W_4$ ), which is closely followed by  $W_3$  (0.55),  $W_9$  (0.51), and  $W_6$  (0.73), as observed for  $FS_W$ . Watershed  $W_1$  and  $W_2$  show an  $FS_W^{A_I}$  of 0.89 and 1.68 (the highest of the GTM), which are higher than their respective values of  $FS_W$ . Finally, watersheds  $W_5$ ,  $W_7$ , and  $W_8$  show values of  $FS_W^{A_I}$  ranging between ~1 and ~1.3.

Finally, Fig. 5C shows the spatial distribution of filtration services at the reef scale per unit of reef area  $(FS_R^{A_R})$ , expressed in  $[\% \text{ km}^{-2}]$ , and its average value for each watershed. Once again,





**Fig. 3** Each plot shows the number of particles located in each of the nine major watersheds divided by their initial number as a function of time. The red circle indicates when the number of particles

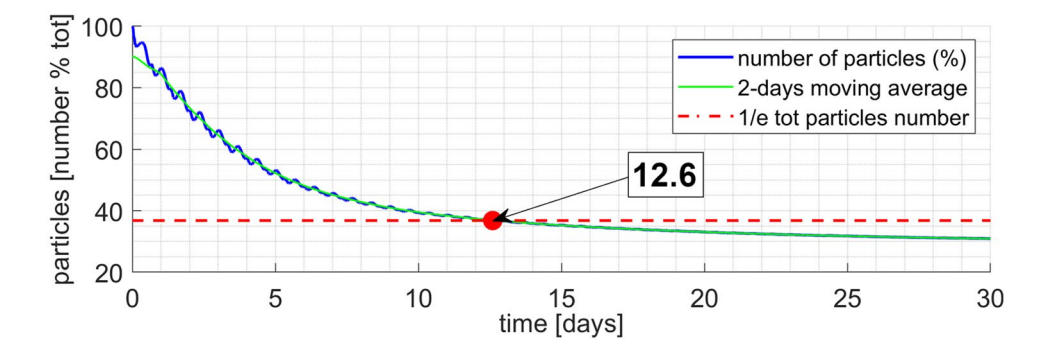
reaches 1/e of the initial value, which is the watershed-scale residence time  $(RT_W)$ . The white boxes contain the value of the residence time expressed in days

the distribution of the values differs from the once observed for  $FS_W$ . The lowest  $\overline{FR}_R^{A_R}$  were observed for the watersheds containing the inlets ( $W_4$  and  $W_7$ ). The highest ones (> 30) were obtained for the watersheds containing Tolomato River ( $W_1$ ) and Salt Run ( $W_5$ ). The values observed for the remaining watersheds range between 15 and 25.

# **Spatial Distribution of the Oyster Reefs**

Figure 5D shows the spatial distribution of the percentage of intertidal watershed area occupied by oyster reefs

Fig. 4 The plot shows the number of particles located in the estuary divided by their initial number as a function of time. The red circle indicates the time at which the number of particles reaches 1/e of the initial value. That time is our estimate of the estuary-scale residence time  $(RT_E)$ . The white box contains the value of the residence time expressed in days





 $(A_R^I)$  at the watershed level. The figure shows that in the watersheds containing Matanzas  $(W_{6-8})$  and Guana River  $(W_2)$ , more than ~5% of the intertidal area is occupied by oyster reefs. The peak value, equal to 11.16%, is observed in watershed  $W_8$ , which contains Matanzas inlet. At the antipode, watershed  $W_4$ , which contains St. Augustine inlet, shows the lowest value of  $A_R^I$ , equal to 1.84%. In the remaining watersheds,  $A_R^I$  ranges between ~2.4 and 3.0%.

**Table 1** Watershed, subestuary, and subpopulation characteristics within the Guana-Tolomato-Matanzas (GTM estuary). Filtration services represent the percent of the GTM estuary that is filtered in by each subestuary. Mean dry tissue weight (DTW) is in grams

| Watershed          | Subestuary<br>volume (1000<br>m <sup>3</sup> ) | Temp (C)     | Mean shell<br>length<br>(mm)<br>[DTW] | Mean reef<br>density<br>(ind./m <sup>2</sup> of<br>reef) | Reef area (1000 m <sup>2</sup> ) | Mean oyster<br>abundance<br>(ind./m² of<br>subestuary) | Mean FR <sub>O</sub> (l/(h*ind.)) | $FR_g$ (1/     | Filtration<br>services<br>( % filtered) |
|--------------------|--|--------------|---------------------------------------|--|----------------------------------|--|-----------------------------------|----------------|---|
| 1                  | 44,100   | 23.97        | 31.90<br>[0.138]                      | 1811.5   | 552                              | 33.07  | 2.18                              | 16.1           | 20.16                                   |
| 2                  | 2380   | 25.48        | 48.52<br>[0.294]                      | 1689.9   | 173                              | 90.19  | 3.74                              | 13.4           | 4.20                                    |
| 3                  | 4050   | 24.65        | 33.71<br>[0.154]                      | 2074.1   | 80                               | 51.56  | 2.45                              | 16.1           | 1.49                                    |
| 4                  | 13,000   | 23.77        | 32.05<br>[0.140]                      | 1811.5   | 22                               | 11.77  | 2.18                              | 15.6           | 0.28                                    |
| 5                  | 4490   | 25.18        | 34.46<br>[0.160]                      | 1939.9   | 59                               | 34.35  | 2.61                              | 16.9           | 2.46                                    |
| 6                  | 21,100   | 24.43        | 36.82<br>[0.181]                      | 1422.2   | 399                              | 49.46  | 2.69                              | 14.9           | 6.07                                    |
| 7                  | 15,500   | 25.19        | 31.92<br>[0.139]                      | 1741.6   | 441                              | 64.22  | 2.42                              | 17.5           | 10.12                                   |
| 8                  | 11,800   | 24.37        | 38.70<br>[0.197]                      | 1249.6   | 960                              | 99.88  | 2.81                              | 14.2           | 9.23                                    |
| 9                  | 9900   | 24.02        | 27.14<br>[0.101]                      | 2940.0   | 168                              | 39.31  | 1.83                              | 18.2           | 4.16                                    |
| Average<br>(STDEV) | 1.400E+10<br>(1.279E+10)                       | 24.56 (0.61) | 35.02 (6.03)<br>[0.167<br>(0.05)]     | 1855.4<br>(473.5)  | 317<br>(3.04E+05)                | 52.65<br>(28.18)                                       | 2.54<br>(0.54)                    | 15.7<br>(1.57) | Total <i>FS</i> = 58.17                 |

# **Genetic Algorithm**

Table 2 shows the value of the statistical parameters obtained for each predictor in Eq. (16), when they were used individually as predictors in a linear regression describing  $FS_R^{A_R}$ , assuming that the other parameters in (16) are constant. The statistical parameters show that the effects of  $\overline{FR}_R^{A_R}$ ,  $RT_R$ , and N on the reef-scale  $FS_R^{A_R}$  were negligible. Notice that for  $\overline{FR}_R^{A_R}$ , the calculated p value was lower than 0.005, indicating statistical significance; however, the low  $R^2$  and the high RMSE and MAE confirmed the negligible contribution of this predictor. For N and  $RT_R$ , both p values were greater than 0.05, and the almost null  $R^2$  confirm their negligible contribution to identify a relationship describing  $FS_R^{A_R}$ . The best predictor of  $FS_R^{A_R}$  was  $\overline{C}$  as it was both highly significant (pvalue < 0.005) and explained more than one-fourth of the variability ( $R^2 = 0.257$ ). This relationship suggested that the  $FS_R^{A_R}$  were influenced by downstream effects in the estuary, because  $\overline{C}$  accounts for the filtration history of the particles. This was confirmed by the value of RMSE, which was the lowest calculated among single predictors models (72.82). Additionally, the value of MAE was comparable to the ones obtained for the other predictors (29.41 vs. 34.05, 33.96, and 34.77), indicating that the relationship obtained from  $\overline{C}$  to describe  $FS_R^{A_R}$  reduces the

variance of the distribution of error magnitudes, but not the average magnitude of the errors.

When the model predictors in Eq. (16) were used in the GA to determine a relationship describing  $FS_R^{A_R}$ , the GA suggested the following relationship:

$$FS_R^{A_R} = a_1 \left( N \cdot \overline{C} \cdot \overline{FR}_R^{A_R} \right) + a_0. \tag{18}$$

Using the numerical model, we observed that, when the number of distinct particles entering a reef (N), their average concentration  $(\overline{C})$ , and the filtration rate of a reef per unit of reef area  $(\overline{FR}_R^{A_R})$  are null,  $FS_R^{A_R}$  is null. Thus, the regression must be performed by setting  $a_0 = 0$  to avoid a wrong estimation of the reef-scale FS, and consequently, the wrong estimation of the estuary scale FS, especially in scenarios where a high number of reefs are not reached by particles floating in the estuary (i.e., neap tides and localized injection of pollutant). We obtained a value of  $a_1$  equal to 7.1535. Table 2 shows the value of the statistical parameters obtained for this relationship. This full model was both highly significant (p value < 0.005) and had much greater explanatory power ( $R^2 = 0.897$ ) than any single-parameter model (Fig. 6). The RMSE and the MAE decreased to 27.97 and 12.11 respectively, showing a strong reduction of the prediction error.



Fig. 5 A Filtration services at the reef scales  $(FS_R)$  and the watershed scale  $(FS_W)$  for each watershed  $(W_i, i=1,9)$ . Both FS are reported in percentage of estuary filtered within a residence time [%]. B The spatial distribution of  $FS_W$  per square kilometer of intertidal watershed area  $(FS_W^{A_I})$ . For each watershed  $(W_i, i=1,9)$ , the values are reported in percentage per square kilometer of intertidal area of the watershed [%/ km<sup>2</sup>]. C The spatial distribution of the filtration services at the reef scale per unit of reef area  $(FS_R^{A_R})$ , and its average values per each watershed  $(\underline{FS}_R^{A_R})$ . For each watershed  $(W_i, i=1,9)$ , the values are reported in percentage per square kilometer of reef area [%/km<sup>2</sup>]. **D** The spatial distribution of the percentage of intertidal watershed area occupied by oyster reefs  $(A_R^I)$ . The values are reported in %

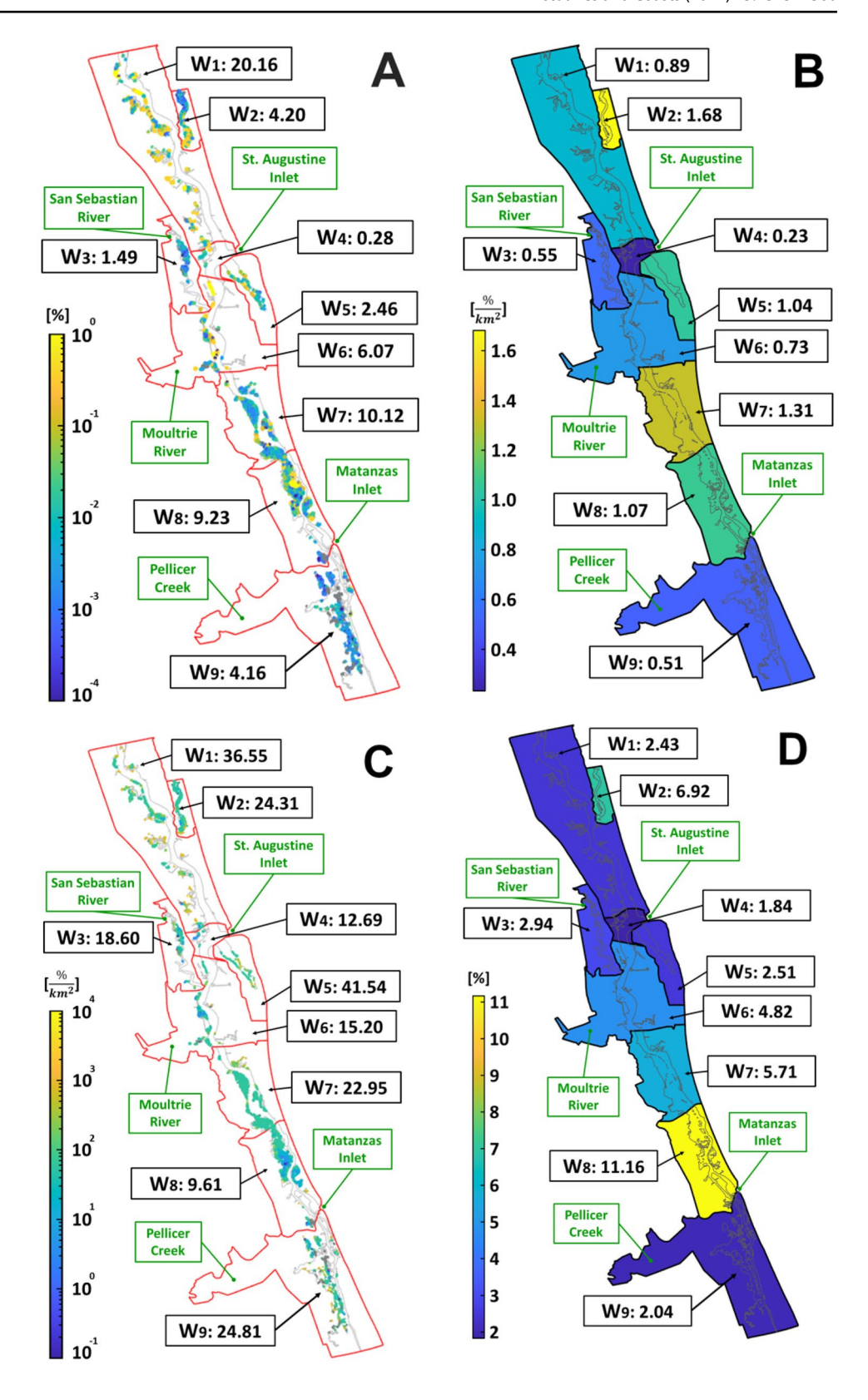




**Table 2** For each single predictor are reported the p value,  $R^2$ , RMSE root mean square error, and MAE mean average error calculated from the relationships obtained from the genetic algorithm to describe  $FS_{R}^{A_R}$ . The relationships are obtained by using each predictor described in the Statistical Analysis section, individually. A full, multiplicative model was obtained by considering most predictors described in the GA

| Predictor  | p value | $R^2$  | RMSE  | MAE   |
|--|---------|--------|-------|-------|
| $\overline{FS}^{A_R}$                              | < 0.005 | 0.0024 | 84.36 | 34.05 |
| RT   | 0.878   | 0.0047 | 84.26 | 33.96 |
| $\overline{C}$                                     | < 0.005 | 0.257  | 72.82 | 31.53 |
| N  | 0.249   | 0.0013 | 86.20 | 34.77 |
| $N \times \overline{C} \times \overline{FS}^{A_R}$ | < 0.005 | 0.897  | 27.97 | 12.11 |

# **Discussion**

The native oyster population in GTM is exceptionally intact and robust when compared to many other populations in the USA and elsewhere that are either in poor condition or functionally extinct (Beck et al. 2011). Importantly, our ability to describe this population and estimate the ecosystem services conferred by this population was bolstered by detailed surveys of 240 randomly selected reefs of the approximately 4,300 in this system, which supplied demographic and density information across all watersheds and subestuaries.

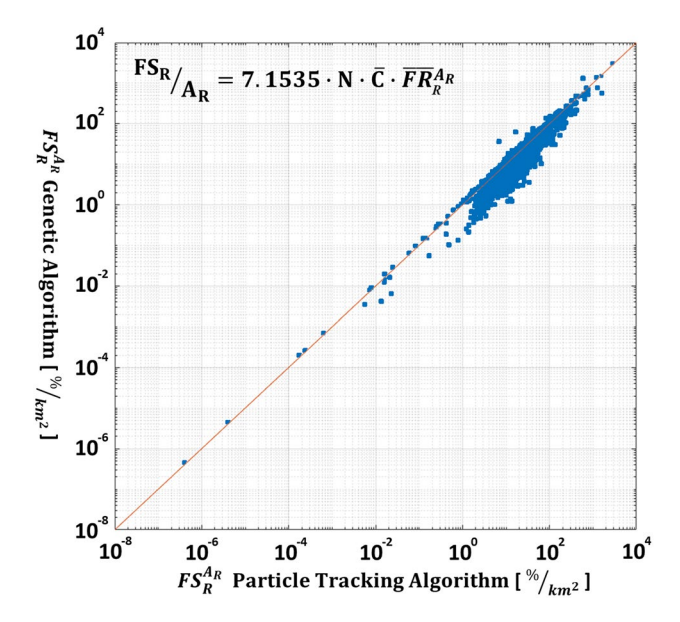


**Fig. 6** Scatter plot comparing the values of the FSRAR obtained from the MATLAB algorithm based on the particle tracking model (x-axis) and the FSRAR obtained from the relationship obtained from the genetic algorithm (y-axis). The relationship is reported in the figure. Both axes are on a logarithmic scale to enhance the visibility of the point cloud

Furthermore, because we could resolve how services varied among populations after controlling for reef size, we could both determine which populations were most efficient at filtering particulate and tease apart the role of various hydrodynamic factors governing filtration services. These types of analyses can inform future management of these populations and the preservation of their valuable services. For example, model results can be used to guide restoration to areas that are more likely to refilter upstream water and thus contribute greater FS. Additionally, conservation efforts should prioritize watershed or reefs that already contribute significant FS at the estuary scale (Fig. 5). The utility of this approach may encourage managers elsewhere to develop their own models to elucidate areas where oysters would be most effective at improving water quality.

For comparative purposes, we specifically chose to estimate the filtration rates of C. virginica by following the approach of zu Ermgassen et al. (2013b), who modeled the current and historic filtration services of this species throughout the Atlantic and Gulf Coasts of the USA. Although our approach to modeling the physical interactions between populations and suspended particles differs significantly between these studies, comparing the results of these studies helps illustrate how the filtration services estimated for present-day GTM populations surpassed those of all contemporary and historic populations. Indeed, among the 13 estuaries modeled estimated by zu Ermgassen et al. (2013b), the maximum filtration services were estimated to be contributed by historic populations in Matagorda Bay during the Fall (51% bay filtered within a residence time). All other peak filtration service estimates among the other historic populations were much less apparent (mean: 4.5%) and present day services among these same populations were on average a small fraction of the historic services (-71% of historic value). The impressive filtration services of oysters in the GTM estuary, along with relatively short residence times (Phlips et al. 2004), likely play a major role in keeping phytoplankton biomass low and providing resilience to natural and human disturbances (Dix et al. 2013).

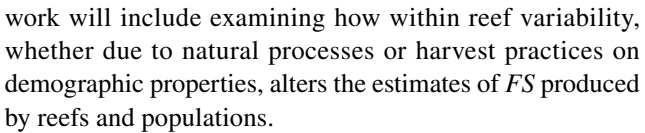
The estimated population metrics and reef-scale biofiltration rates underpinning the ecosystem scale results are also worth examining. Reefs were dominated by relatively small individuals (mean shell height = 35.02 mm) due to persistent annual recruitment; however, oyster densities within reefs were also quite high (mean = 1855 ind./m²) and relative abundance of these populations within subestuaries (mean = 52 ind./m² of estuary) was relatively high compared to historic coverage across the 13 estuaries (mean historic oyster coverage: 36.6 ind./m²) examined by zu Ermgassen et al. (2013b).

It is important to note that we only account for oyster filtration services within this model while neglecting those reef community members that also contribute to filtration



services. Indeed, other GTMNERR survey data indicated a strong relationship between oysters and other suspension feeders including ribbed mussels ( $R^2 = 0.69$ ) and regular presence of other filter-feeding invertebrates (i.e., quahog clams, barnacles, mahogany date mussels) (Marcum et al. 2018). Non-oyster suspension feeders on reefs can add appreciably to total reef biomass (e.g., ~16%) and contribute significantly to biofiltration and water quality improvement (Kellogg et al. 2013). That said, the relatively common filtration rates estimated here (mean 2.54 l h<sup>-1</sup>) combined with the high density of oysters on reefs produced reef-scale filtration rates (mean  $FS_R^{A_R}$ : 4,136 1 h<sup>-1</sup> m<sup>2</sup>) that were orders of magnitude greater than maximum filtration rates indirectly measured on natural (44 1 h<sup>-1</sup> m<sup>2</sup>) and constructed (154 1/h/ m<sup>2</sup>) reefs in the Gulf of Mexico; albeit these reefs were much less dense (407 ind. m<sup>-2</sup> and 690 ind. m<sup>-2</sup>, respectively) than those found in GTM (Milbrandt et al. 2015). Nevertheless, we are confident that if other community members were included, it would not be surprising to observe our reef-scale filtration estimates increase substantially. The large estimates for  $FS_R^{A_R}$  in GTM are not without precedent and resemble the maximum (summer = 26 °C) filtration rates estimated for pre-colonial reefs in the Chesapeake Bay with a maximum age between 14 years and (3,872 1 h<sup>-1</sup> m<sup>2</sup>) and 16 years old  $(5,388 \text{ 1 h}^{-1} \text{ m}^2)$  (Mann et al. 2009). Maximum filtration rates are appropriate to use in this comparison as the average temperature in each subestuary of the GTM in the model (~24.5 °C) approached that which elicits maximal feeding responses of C. virginica (e.g., 26 °C Newell et al. 2005, 27 °C zu Ermgassen et al. 2013b; Cerco and Mark 2005).

In many previous models of oyster filtration services, the density, demographics and precise spatial distribution of reefs (historic or otherwise) are unknown and many assumptions about the access populations have to overlying water must be simplified during model creation (e.g., Pomeroy et al. 2006; Fulford et al. 2010; zu Ermgassen et al. 2013; zu Ermgassen et al. 2013b). Our approach overcame this limitation by using a coupled FWRI+GTMNERR dataset, which contained detailed and up-to-date spatial and biological information of the reefs in the study area. However, while the FWRI dataset contains the spatial location and the extension of all the known reefs occupied by living oyster communities in the GTM estuary, the biological information in the GTMNERR dataset of area were available only for a limited number of reefs (~6% of total reefs). We verified the accuracy of the IDW interpolation method used here to estimate the biological properties of the oysters in unsurveyed reefs, by excluding 20 reefs and using them to compute the error. MAE and RMSE were equal to 6.3 and 6.1 mm for the shell height, and to 578.6 and 310.3 oysters/m<sup>2</sup>. This was due to a fairly uniform distribution of the surveys, which spanned the whole GTM estuary and its tributaries. Future



Because of the high computational cost of numerically tracking particles over each reef in large domains, researchers developed simplified methods to evaluate oyster FS based on coarse regular grids (e.g., Gray et al. 2019). The use of these grids has two major drawbacks: (i) the boundaries of a naturally irregular reef morphology cannot adequately be described by a coarse regular grid; (ii) particles entering a coarse cell can be filtered even if they do not directly travel over the reef (Figure A1). To overcome these drawbacks, our approach modeled the hydrodynamic in the complex GTM estuary using a high-resolution curvilinear grid, which follows the main watercourses, coupled with high-resolution elevation data, obtained from open datasets and targeted local surveys. More importantly, our model filtered only the particles traveling over the reefs in the GTM estuary. The small increase in the computational costs related to this method was completely justified by the improvement in the description of the filtration history of the tracked particles.

# **Residence Time**

In this study, to evaluate the relationship between the filtration services and the residence time, we calculated the latter at different spatial scales (e.g., local, watershed, estuary). However, our results underlined the absence of a strong relationship between the filtration services and the residence time in the study area. A literature review revealed that no authors calculated the residence time at the local scale in the GTM estuary. At the local scale, the residence time was higher in the salt marshes than in the main channels, due to the lower water fluxes. On the marsh platform, the residence time is maximum toward its landward boundary, where water fluxes are minimal, and progressively decreases close to the marsh edge due to the water exchange with tidal flats and channels flanking the marsh. Also in the main channels, the residence time continues to reduce approaching the inlets, due to the progressive increase of the water fluxes. We observed relatively higher residence times in the southern part of the GTM estuary. This is due to the smaller cross-section of the Matanzas River, in comparison with the Tolomato River, the larger extension of salt marshes in the southern part of the estuary, and the shallow depths at Matanzas inlet, which reduce tidal exchange with the sea.

At the watershed scale, the residence times we calculated in the GTM generally agree with the ones calculated Sheng et al. (2008). Slight differences are obtained because in Sheng et al. (2008): (i) the watersheds do not perfectly match the ones we used in this study; (ii) the residence time is calculated as the time needed to remove the 50% of the



pollutants from an area. In this study, instead, we used ~65% as a threshold; (iii) the numerical grid they used to compute the residence time did not contain the salt marshes and the major creeks that empty into the estuary, as we did. This addition allows us to discover a relationship between the extension of the intertidal  $(A_I)$  and subtidal  $(A_S)$  areas, and the length  $(L_N)$  of the primary tidal network (main channels and rivers), with the residence time. All the variables are calculated at the watershed scale.

We then analyzed this relationship by performing a linear regression. The results and the regression formula are reported in Fig. 8. The  $R^2$  and SD are equal to 0.66, 7.85 days respectively. The results indicate that  $RT_W$  increases with the intertidal area, and the length of the watershed-scale tidal network, and decreases with an increase in subtidal area. Thus, the lowest  $RT_W$  was observed for watersheds  $W_4$ , due to the limited extension of this basin, the consequent low value of the regression variables  $(A_I, A_S, \text{ and } L_N)$ , and the strong tidal dominance of the basin (see the large oscillations in Fig. 3F), due to the proximity to St. Augustine inlet. A higher  $RT_W$  is observed for watersheds  $W_2$ ,  $W_3$ ,  $W_5$ , and  $W_7$ , due to the larger subtidal area, and the longer extension of the tidal network of these watersheds in comparison with  $W_4$ . A relatively high  $RT_W$  is observed for  $W_8$ , due to the numerous salt marshes located in the watershed and the longer tidal network, which bifurcates ~3 km from the inlet. Another reason is the lower fluxes moving through the shallow Matanzas inlet compared to St. Augustine inlet, and the lower tidal dominance compared to  $W_4$  (see the small oscillations in Fig. 3H). Very high values are observed for  $W_1$  and  $W_9$ , due to the presence of the Tolomato River and Pellicer Creek, and to the wide salt marshes surrounding them. In  $W_1$ , the effect of the massive intertidal area on  $RT_W$  is mitigated by the strong fluxes in the Tolomato River. Finally, the greatest  $RT_W$  was computed for watershed  $W_6$ , due to the large shallow areas constituting the border of the Matanzas River and Moultrie Creek, which trap the particles used in this study, limiting their removal from the watershed. Some

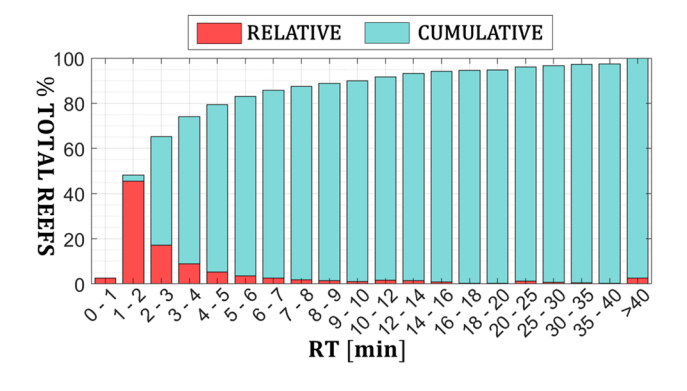


Fig. 7 Relative (red) and cumulative (teal) frequency distribution of the residence time calculated for the reefs in the estuary

of these results are confirmed by Phlips et al. (2004), who indicated higher residence times for Pellicer Creek and Tolomato River and lower residence times for the areas adjacent to Matanzas and St. Augustine Inlets.

To conclude, the estuary scale residence time confirmed the value observed by Sheng et al. (2008) in the region (~14 days).

# **Numerical Approach**

To mechanistically understand the drivers of the observed values of  $FS_W$ , we broke  $FS_W$  down into different terms. Our results underline that  $FS_W$  increases with the intertidal area of the watershed, the average FS of the reef per unit reef  $\overline{FS}_R^{A_R}$ , and the area of oyster reefs per unit of wetted watershed  $A_R^I$ . To remove the dependency of FS on the dimension of the area used for their computation, reef- and watershed-scale filtration services we divided them by the respective areas. Computing the values of the various FS per unit area allowed us to (i) compare the relative contribution of each reef and watershed to  $FS_E$ , and (ii) identify which region of the estuary can provide the maximum increase in  $FS_E$  if targeted for restoration. In short, FS per unit area described the filtering efficiency of reefs and watersheds.

The relationship obtained from the GA suggests that the average initial concentration (C) of the particles entering a reef, as well as their number (N), was more important than their permanence  $(RT_R)$  over the reef. The limited importance of  $RT_R$  was due to its limited variability observed over the reefs. In fact,  $\sim 80\%$  of the reefs showed an  $RT_R$  between 1 and 5 min (Fig. 7). Similarly, the average concentration had a greater impact than the average mass of the particles entering a reef. This was because C accounted for the dilution of the particulate in the seawater volume above the reefs, which highly influenced the FS of the reef  $(FS_R)$ . The good prediction capabilities of  $\overline{C}$  were confirmed by the statistical parameters reported in Table 2. Moreover, we wish to highlight that the value of  $\overline{C}$  depends on the following: (i) the number of reefs crossed by the particles throughout the estuary. This number, in turn, depended on the localand estuary-scale hydrodynamics, the initial distribution of particles injected in the estuary, and the spatial distribution of estuary reefs; (ii) the local reef filtration rate per unit of area  $(FR_R^{-R})$ , which in turn depended on the local oyster population characteristics. Thus, by considering  $FR_R^{-\kappa}$ , Eq. (18) underpinned the importance of the oyster reef properties in the resulting FS. Finally, although the model was initiated with uniformly distributed particles over the GTM, downstream effects were not uniformly distributed. For this reason, in the GTM, the oyster reef contribution to water quality depended on their spatial arrangement and upon the estuary hydrodynamics.



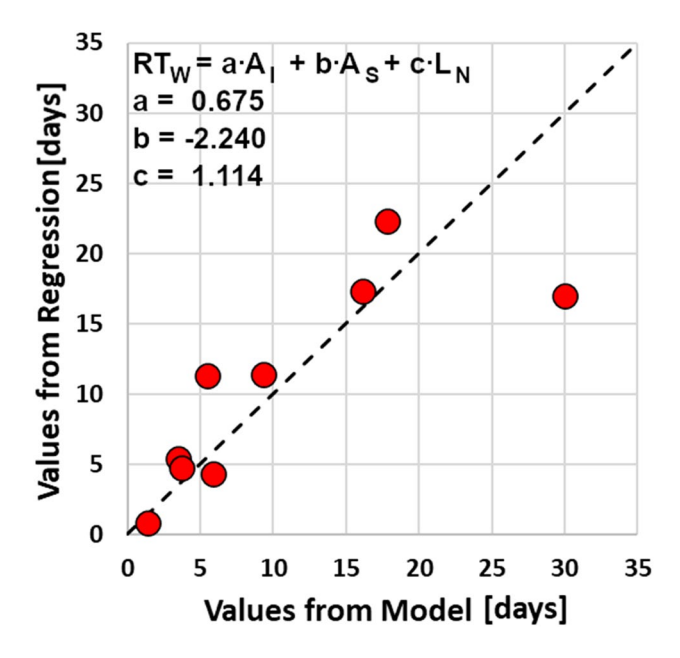
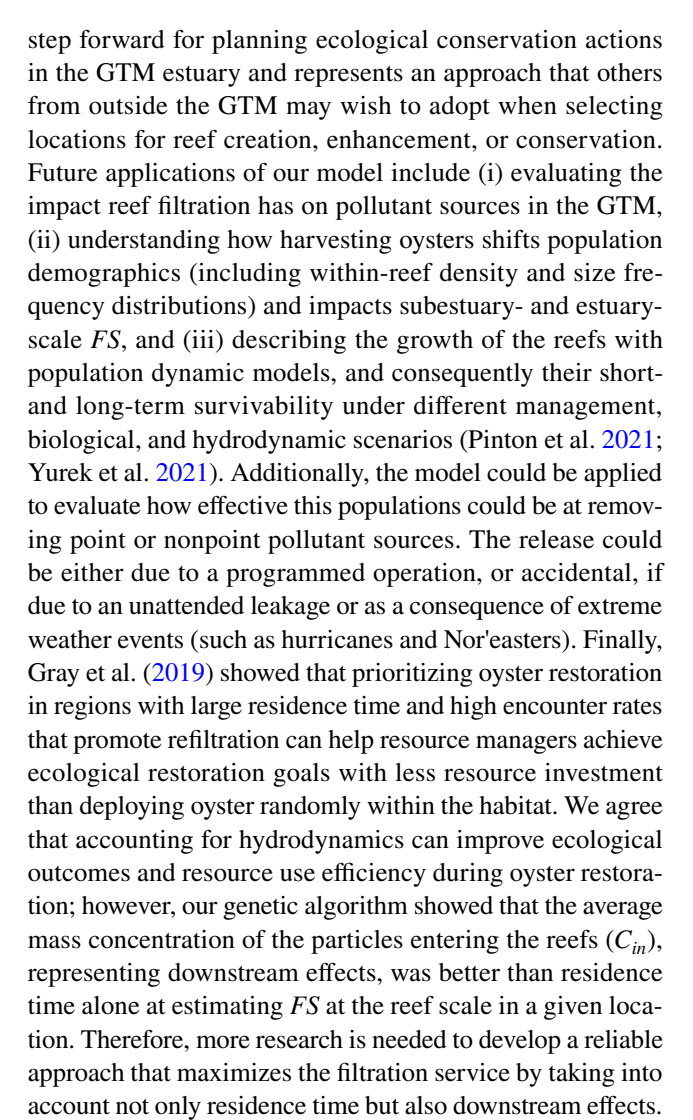


**Fig. 8** Scatter plot comparing the residence times we calculated from the numerical model, on the 9 watersheds constituting the GTM, and the ones obtained from the linear regression we performed by using as variables the extension of the intertidal  $(A_I)$  and subtidal  $(A_S)$  areas, and the length  $(L_N)$  of the primary tidal network (main channels and rivers) in the watersheds

By identifying a clear correlation between the concentration of water parcels traveling over an oyster reef and the reef FS, we showed that downstream effects directly influenced FS, and have to be explicitly considered when planning restoration if water quality improvement is a major project goal. Restoring oysters by prioritizing locations with relatively high residence time as in Gray et al. (2019) might not always be the exclusive best strategy. Our study indicated the optimal locations for targeted restoration were determined by taking into account both residence time and water refiltration through downstream effects, which can only be accomplished with precise spatial knowledge of oyster locations, abundance, and hydrological patterns. Note that we used uniformly distributed particles over the GTM to make the results obtained for each reef in the estuary independent of the initial position of the particles. However, the reef- and the watershed-scale FS calculated for the GTM had a nonuniform distribution due to the complex local and estuaryscale hydrodynamics. A high-resolution modeling approach was then needed to precisely describe the GTM hydrodynamics and to correctly estimate the contribution of oyster reefs to estuarine water quality.

# **Future Developments**

We estimated the local contribution of individual reefs to the global (i.e., estuary-scale) FS. This is a fundamental



#### **Conclusions**

In this work, we used a numerical model that solved hydrodynamics and transport of particulate matter to estimate oyster filtration service of Eastern oysters (C. virginica) in the GTM estuary, FL, which possess traits (reef density, oyster abundance, etc.) that may resemble "pristine" populations that were more common in the USA prior to arrival of Euro-American settlers. By tracking the time spent by each particle over a reef, the model accounted for the mass removed from the particles floating over the reefs. Accounting for reef area when estimating FS provided novel insight of the relative contribution of reefs, which can provide valuable resource management information. The model results show that: (i) oyster reefs populating the GTM improved water quality by filtering ~60% of the estuary's volume within a single residence time; (ii) the spatial distribution of the filtration service at the reef and watershed scales varied spatially



across estuary; (iii) at the watershed scale, FS depended on the distribution of the reefs in the watershed and on the proportion of the wetted watershed area they occupy. Finally, our genetic algorithm revealed that the average mass concentration of the particles entering the reefs  $(\overline{C})$ , a proxy for downstream effects), rather than residence time, best described the reef-scale contribution to estuary-scale FS. In future research projects, we intend to apply the model in a variety of ways to explore how natural and anthropogenic effects influence FS at any scale.

**Supplementary Information** The online version contains supplementary material available at https://doi.org/10.1007/s12237-021-01017-x.

**Funding** This research was partially funded by NSF BIO-OCE Award 1736943 to DLK.

# References

- Akaike, Hirotugu. 1973. Information theory and an extension of the maximum likelihood principle. In *Second international symposium on information theory* 267–281. Budepest.
- Allen, Steve, A. C. Carpenter, M. W. Luckenbach, Kennedy T. Paynter Jr, Angela Sowers, Eric Weissberger, James A. Wesson, and Stephanie Westby. 2011. Restoration Goals, Quantitative Metrics and Assessment Protocols. Report of the Oyster Metrics Workgroup. Chesapeake Bay Program.
- Atlantic States Marine Fisheries Commission. 2007. The importance of Habitat Created by Shellfish and Shell Beds Along the Atlantic Coast of the US Washington. DC.
- Bacopoulos, Peter, Amanda S. Tritinger, and Nicole G. Dix. 2019. Sea-level rise impact on salt marsh sustainability and migration for a subtropical estuary: GTMNERR (Guana Tolomato Matanzas National Estuarine Research Reserve). Environmental Modeling & Assessment 24: 163–184. https://doi.org/10.1007/s10666-018-9622-6.
- Beck, Michael W., Robert D. Brumbaugh, Laura Airoldi, Alvar Carranza, Loren D. Coen, Christine Crawford, Omar Defeo, et al. 2011. Oyster reefs at risk and recommendations for conservation, restoration, and management. *BioScience* 61: 107–116. https://doi.org/10.1525/bio.2011.61.2.5.
- Cerco, C., and Mark R. Noel. 2005. Assessing a ten-fold increase in the Chesapeake Bay native oyster population. Report to EPA Chesapeake Bay Program. Annapolis, Maryland, USA: US Army Engineer Research and Development Center, Vicksburg MS.
- Coen, Loren D., and Austin T. Humphries. 2017. Their services, enhancement, restoration and monitoring. In *Routledge handbook of ecological and environmental restoration*, ed. Stuart K. Allison and Stephen D. Murphy, 274–294. Taylor & Francis.
- Coen, Loren D., Robert D. Brumbaugh, David Bushek, Ray Grizzle, Mark W. Luckenbach, Martin H. Posey, Sean P. Powers, and S. Gregory Tolley. 2007. Ecosystem services related to oyster restoration. *Marine Ecology Progress Series* 341: 303–307.
- Cranford, Peter J. 2019. Magnitude and extent of water clarification services provided by bivalve suspension feeding. In *Goods and Services of Marine Bivalves*, ed. Aad C. Smaal, Joao G. Ferreira, Jon Grant, Jens K. Petersen, and Øivind Strand, 119–141. Cham: Springer International Publishing. https://doi.org/10.1007/978-3-319-96776-9\_8.
- Cranford, Peter J., J. Evan Ward, and Sandra E. Shumway. 2011. Bivalve filter feeding: variability and limits of the aquaculture

- biofilter. In *Shellfish Aquaculture and the Environment*, ed. Sandra E. Shumway, 81–124. Wiley-Blackwell.
- Dix, Nicole G., A. Noel, H. J. Brockmeyer, H. J. Cho, S. R. Allen, and K. R. Radabaugh. 2017. Northeast Florida. In Coastal Habitat Integrated Mapping and Monitoring Program Report for the State of Florida, ed. K. R. Radabaugh, C. E. Powell, and R. P. Moyer. 21. Florida Fish and Wildlife Conservation Commission Fish and Wildlife Research Institute.
- Dix, Nicole, Edward Phlips, and Peter Suscy. 2013. Factors controlling phytoplankton biomass in a subtropical coastal lagoon: relative scales of influence. *Estuaries and Coasts* 36. *Coastal and Estuarine Research Federation*: 981–996.
- Dix, Nicole G., L. Walters, E. Hernandez, A. Roddenberry, S. Garvis, M, and Anderson, K. R. Radabaugh. 2019. Northeast Florida. In Oyster Integrated Mapping and Monitoring Program Report for the State of Florida, ed. K.R. Radabaugh, R.P. Moyer, S.P. Geiger. 22. Florida Fish and Wildlife Conservation Commission Fish and Wildlife Research Institute.
- Filgueira, Ramón, Thomas Guyondet, Luc A. Comeau, and Réjean. Tremblay. 2016. Bivalve aquaculture-environment interactions in the context of climate change. *Global Change Biology* 22: 3901–3913. https://doi.org/10.1111/gcb.13346.
- Fulford, Richard S., Denise L. Breitburg, Mark Luckenbach, and Roger I. E. Newell. 2010. Evaluating ecosystem response to oyster restoration and nutrient load reduction with a multispecies bioenergetics model. *Ecological Applications* 20: 915–934. https://doi.org/ 10.1890/08-1796.1.
- Fulford, Richard S., Denise L. Breitburg, Roger IE. Newell, and WMichael Kemp, and Mark Luckenbach. 2007. Effects of oyster population restoration strategies on phytoplankton biomass in Chesapeake Bay: A flexible modeling approach. *Marine Ecology Progress Series* 336: 43–61.
- Gerritsen, Jeroen, A. Frederick Holland, and David E. Irvine. 1994. Suspension-feeding bivalves and the fate of primary production: An estuarine model applied to Chesapeake Bay. *Estuaries* 17: 403–416. https://doi.org/10.2307/1352673.
- Gray, Matthew W., and Chris J. Langdon. 2018. Ecophysiology of the Olympia Oyster, Ostrea lurida, and Pacific Oyster, *Crassostrea gigas*. *Estuaries and Coasts* 41: 521–535. https://doi.org/10.1007/s12237-017-0273-7.
- Gray, M., and Philine zu Ermgassen, Jonathan Gair, Chris Langdon, Emily Lemagie, and Jim Lerczak. 2019. Spatially explicit estimates of in situ filtration by native oysters to augment ecosystem services during restoration. *Estuaries and Coasts* 42: 792–805. https://doi.org/10.1007/s12237-019-00515-3.
- Grizzle, R.E., J.K. Greene, and L.D. Coen. 2008. Seston removal by natural and constructed intertidal eastern oyster (*Crassostrea vir-ginica*) reefs: A comparison with previous laboratory studies, and the value of in situ methods. *Estuaries and Coasts* 31: 1208–1220.
- Hernández, Ada Bersoza, Robert D. Brumbaugh, Peter Frederick, Raymond Grizzle, Mark W. Luckenbach, Charles H. Peterson, and Christine Angelini. 2018. Restoring the eastern oyster: How much progress has been made in 53 years? Frontiers in Ecology and the Environment 16: 463–471. https://doi.org/10.1002/fee.1935.
- Jacobs, P., K. Troost, R. Riegman, and J. van der Meer. 2015. Lengthand weight-dependent clearance rates of juvenile mussels ( Mytilus edulis ) on various planktonic prey items. Helgoland Marine Research 69. BioMed Central: 101–112. https://doi.org/10.1007/ s1-152-014-0419-y
- Kellog, M. Lisa., Jeffrey C. Cornwell, Michael S. Owens, and Kennedy T. Paynter. 2013. Denitrification and nutrient assimilation on a restored oyster reef. *Marine Ecology Progress Series* 480: 1–19. https://doi.org/10.3354/meps10331.
- Kurlansky, Mark. 2007. The big oyster: History on the half shell. Random House.



- Lemagie, Emily P., and James A. Lerczak. 2015. A comparison of bulk estuarine turnover timescales to particle tracking timescales using a model of the Yaquina Bay estuary. *Estuaries and Coasts* 38: 1797–1814.
- Madár, János, János Abonyi, and Ferenc Szeifert. 2005. Genetic programming for the identification of nonlinear input- output models. *Industrial & engineering chemistry research* 44. ACS Publications: 3178–3186.
- Mann, Roger, and Eric N. Powell. 2007. Why oyster restoration goals in the Chesapeake Bay are not and probably cannot be achieved. *Journal of Shellfish Research* 26: 905–917.
- Mann, Roger, Juliana M. Harding, and Melissa J. Southworth. 2009. Reconstructing pre-colonial oyster demographics in the Chesapeake Bay, USA. *Estuarine, Coastal and Shelf Science* 85: 217–222. https://doi.org/10.1016/j.ecss.2009.08.004.
- Marcum, Dix P., and M. Monroe. 2018. *Oyster Monitoring Summary*. Guana Tolomato Matanzas National Estuarine Research Reserve.
- Milbrandt, E.C., M. Thompson, L.D. Coen, R.E. Grizzle, and K. Ward. 2015. A multiple habitat restoration strategy in a semi-enclosed Florida embayment, combining hydrologic restoration, mangrove propagule plantings and oyster substrate additions. *Ecological Engineering* 83: 394–404. https://doi.org/10.1016/j.ecoleng.2015. 06.043.
- NERRS. 2021. NOAA National Estuarine Research Reserve System (NERRS). System-wide Monitoring Program. *Centralized Data Management Office*.
- Newell, R.I.E. 1988. Ecological changes in Chesapeake Bay: Are they the result of overharvesting the American oyster, Crassostrea virginica. Understanding the Estuary: Advances in Chesapeake Bay Research 129: 536–546.
- Newell, R. I. E., and C. J. Langdon. 1996. Mechanisms and physiology of larval and adult feeding. In *The Eastern Oyster Crassostrea virginica*, ed. V. S. Kennedy, R. I. E. Newell, and A. F. Eble, 185–229. College Park, Maryland: Maryland Seagrant.
- Newell R.I.E., Fisher T.R., Holyoke R.R., Cornwell J.C. (2005) Influence of Eastern Oysters on Nitrogen and Phosphorus Regeneration in Chesapeake Bay, USA. In: Dame R.F., Olenin S. (eds) The Comparative Roles of Suspension-Feeders in Ecosystems. NATO Science Series IV: Earth and Environmental Series, vol 47. Springer, Dordrecht. https://doi.org/10.1007/1-4020-3030-4\_6
- Phlips, E. J., N. Love, S. Badylak, P. Hansen, J. Lockwood, C. V. John, and R. Gleeson. 2004. A Comparison of Water Quality and Hydrodynamic Characteristics of the Guana Tolomato Matanzas National Estuarine Research Reserve and the Indian River Lagoon of Florida\*. Journal of Coastal Research SI. Fort Lauderdale, United Kingdom: Allen Press Inc.: 93–109.

- Pinton, D., A. Canestrelli, S. Yurek, and J. Martin. 2021. Growth and collapse of oyster reefs in intertidal flats under different wave climates. New Orleans.
- Pomeroy, Lawrence R., Christopher F. D'Elia, and Linda C. Schaffner. 2006. Limits to top-down control of phytoplankton by oysters in Chesapeake Bay. *Marine Ecology Progress Series* 325: 301–309. https://doi.org/10.3354/meps325301.
- Pomeroy, Lawrence R., Christopher F. D'Elia, and Linda C. Schaffner, et al. 2007. Top-down control of phytoplankton by oysters in Chesapeake Bay, USA: Reply to Newell et al. (2007). *Marine Ecology Progress Series* 341: 299–301. https://doi.org/10.3354/meps341299.
- Roelvink, Dano J.A.., and Dirk-Jan. Walstra. 2005. Keeping it simple by using complex models. *Advances in Hydroscience and Engineering* 6: 11.
- Saraiva, S., L. Fernandes, J. van der Meer, R. Neves, and S.A.L.M. Kooijman. 2017. The role of bivalves in the Balgzand: First steps on an integrated modelling approach. *Ecological Modelling* 359: 34–48. https://doi.org/10.1016/j.ecolmodel.2017.04.018.
- Sheng, Y. Peter, Bilge Tutak, Justin R. Davis, and Vladimir Paramygin. 2008. Circulation and flushing in the lagoonal system of the Guana Tolomato Matanzas National Estuarine Research Reserve (GTMNERR), Florida. Journal of Coastal Research. Coastal Education & Research Foundation, Inc.: 9–25.
- Yang, C., H. Li, Y. Rezgui, I. Petri, B. Yuce, B. Chen, and B. Jayan. 2014. High throughput computing based distributed genetic algorithm for building energy consumption optimization. *Energy and Buildings* 76: 92–101. https://doi.org/10.1016/j.enbuild.2014.02. 053.
- Yurek, S., M. Eaton, R. Lavaud, R.W. Laney, D. DeAngelis, W.E. Pine III., M.K. LaPeyre, et al. 2021. Modeling structural mechanics of oyster reef self-organization including environmental constraints and community interactions. *Ecological Modelling*. https://doi. org/10.1016/j.ecolmodel.2020.109389.
- zu Ermgassen, P., M. D. Spalding, R. E. Grizzle, and R. D. Brumbaugh. 2013a. Quantifying the loss of a marine ecosystem service: Filtration by the eastern oyster in US estuaries. *Estuaries and Coasts* 36: 36–43
- zu Ermgassen, P., M. W. Gray, C. J. Langdon, M. D. Spalding, and R. D. Brumbaugh. 2013b. Quantifying the historic contribution of Olympia oysters to filtration in Pacific Coast (USA) estuaries and the implications for restoration objectives. *Aquatic Ecology* 47: 149–161. https://doi.org/10.1007/s10452-013-9431-6.

